Journal of Power Sources 252 (2014) 144–149

Contents lists available at ScienceDirect

Journal of Power Sources

journal homepage: www.elsevier.com/locate/jpowsour

Facile synthesis of Si nanoparticles using magnesium silicide reduction and its carbon composite as a high-performance anode for Li ion batteries

Yoon Hwa [a], Won-Sik Kim [a], Byeong-Chul Yu [a], Jae-Hun Kim [b], Seong-Hyeon Hong [a], Hun-Joon Sohn [a,*]

[a] Department of Materials Science and Engineering, Seoul National University, Seoul 151-744, Republic of Korea
[b] School of Advanced Materials Engineering, Kookmin University, Seoul 136-702, Republic of Korea

HIGHLIGHTS

- The Si nanoparticles are prepared using mechano-chemical reduction of SiO_2.
- Mg_2Si is used as a reductant.
- Pre-existing MgO nano-particles act as pore generating agents for the formation of mesopores.
- The nano-Si/C electrode exhibited *c.a.* 1600 mAh g^{-1} over 50 cycles at a current of 1.0 A g^{-1}.

GRAPHICAL ABSTRACT

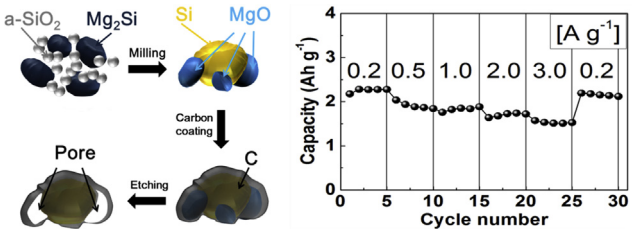

ARTICLE INFO

Article history:
Received 6 November 2013
Received in revised form
28 November 2013
Accepted 30 November 2013
Available online 11 December 2013

Keywords:
Lithium ion battery
Anode
Magnesium silicide
Mechano-chemical reduction
Silicon

ABSTRACT

A new method for a facile synthesis of nano-silicon/carbon mesoporous composite is proposed. Silicon nanoparticles can be obtained through the magnesium silicide reduction of amorphous silica using high energy mechanical milling process. And mesoporous carbon matrix is fabricated *via* simple carbon coating method on Si nanoparticles followed by chemical etching of preexisting magnesium oxide nanoparticles. This nano-silicon/carbon mesoporous composite electrode shows an excellent electrochemical performance as an anode for lithium ion batteries, achieving a reversible capacity of *c.a.* 1600 mAh g^{-1} over 50 cycles at a current of 1.0 A g^{-1} and superior rate capabilities with reversible capacity of about 1530 mAh g^{-1} at a discharge current density of 3 A g^{-1}.

1. Introduction

Si-based electrodes have become a strong candidate to replace the conventional carbon anodes in lithium ion batteries (LIBs), due to their large theoretical capacity at room temperature ($Li_{15}Si_4$, 3600 mAh g^{-1}), which is almost 10 times higher than that of graphite anodes (LiC_6, 372 mAh g^{-1}), as well as a low operating voltage (0.4–0.5 V *vs.* Li/Li^+) [1–3]. Moreover, the abundance and environmentally friendliness of Si are other advantages for use as an electrode material. However, the large capacity of Si for Li accommodation could be a drawback, paradoxically, due to the large volume change of up to 300% for Si particles during the lithiation and delithiation process, which leads to pulverization of the electrode [1]. In addition, a low electrical conductivity of Si due to its semi-conductive nature negatively influences the electrochemical properties when Si is used as an anode material for LIBs. Therefore, these drawbacks should be overcome to use Si-based material as an

* Corresponding author. Tel.: +82 2 880 7226; fax: +82 2 885 9671.
E-mail address: hjsohn@snu.ac.kr (H.-J. Sohn).

0378-7753/$ – see front matter © 2013 Elsevier B.V. All rights reserved.
http://dx.doi.org/10.1016/j.jpowsour.2013.11.118

anode for LIBs [1]. Recently, many researchers have been trying to modify Si-based electrodes through synthesizing unique nano-structures [4–8] and also by using Si/M nano-composite materials (M = electrochemically active or inactive material with Li) [9–19]. The nano-Si/carbon (n-Si/C) mesoporous composite concept is one good approach to achieve excellent electrochemical properties for LIB anode materials. Generally, carbonaceous materials are highly attractive for applications in energy conversion and storage systems such as LIB electrode material [19–21], the supporting matrix for catalysts in fuel cells [22], and electrochemical capacitors [23]. For application as LIB electrode materials, core element/carbon mesoporous composite materials can enhance the electrochemical performance of anode materials [19,20], because mesoporous carbon matrix can act as a buffering matrix against volume change of the core particles by its mesoporous structure during lithiation/delithiation process, and can contribute to maintaining a stable electrical pathway for active material during electrode reaction with Li ions.

The synthesis of nano-sized Si is another important issue, for the application of LIBs to electrical vehicles (EVs) and electronic mobile devices which demand high power and high energy density of the electrode. For this reason, synthesizing Si nanoparticles through the mechano-chemical reduction of amorphous silica (a-SiO_2) using a high-energy mechanical milling (HEMM) process can be a good approach, owing to its capability for facile synthesis. The HEMM process, is widely used in the powder metallurgy industry, and is used effectively in mechanical alloying processes, particle size control, and the synthesis of a composite powder [24]. Sony's Nexelion LIBs anode is a representative electrode material prepared by HEMM methods [25]. In previous work, a mesoporous Si nanoparticles can be obtained easily through the magnesio-mechanochemical reduction of a-SiO_2 using an HEMM process [26]. The reaction chemistry is as follows [26]:

$$SiO_2 + 2\ Mg \rightarrow Si + 2MgO\ (\Delta G^0 = -67.5\ \text{kcal mol}^{-1}, 298\ K) \quad (1)$$

Herein, a new approach for the mechano-chemical synthesis of Si nanoparticles is proposed with magnesium silicide (Mg_2Si) instead of magnesium (Mg) as a reductant. As the Mg reduction of SiO_2 is thermodynamically favorable [26–31], Mg_2Si reduction of SiO_2 is also a thermodynamically feasible reaction. The reaction chemistry of the Mg_2Si reduction of SiO_2 can be expressed as follows:

$$SiO_2 + Mg_2Si \rightarrow 2Si + 2MgO\ (\Delta G^0 = -49.1\ \text{kcal mol}^{-1}, 298\ K) \quad (2)$$

The reduction of SiO_2 with Mg_2Si in Equation (2) would provide twice the amount of Si nanoparticles compared with the Mg reduction of a-SiO_2 described in Equation (1). a-SiO_2 is employed in this study. The n-Si/C mesoporous composite is prepared facilely through the aforementioned Mg_2Si reduction of a-SiO_2, simple carbon coating, and a chemical etching process, in sequence. Poly vinyl alcohol (PVA) is chosen as a carbon matrix precursor, since PVA can be dissolved in distilled water and carbonized easily by a pyrolysis process [18,32]. Meso-pores in carbon matrix can be formed through etching of the unnecessary magnesium oxide (MgO) phase, which is a simple process compared with other processes requiring an additional template material to form a porous structure [19].

2. Experimental

2.1. Synthesis

The n-Si/C mesoporous composite was prepared as follows. Commercial a-SiO_2 (Sigma–Aldrich, amorphous silica) and Mg_2Si powder (Sigma–Aldrich, 20 mesh, 99+ %) at a molar ratio of 1:1 were put into an 80-cm^3 hardened steel vial with stainless steel balls (diameter: 3/8″ and 3/16″) at a ball-to-powder ratio of 20:1 and milled at 900 rpm for 12 h under an Ar atmosphere. Particle size of pristine a-SiO_2 and Mg_2Si powders were approximately 20 nm and 50 μm, respectively. For the preparation of the n-Si/MgO/C composite, 0.2 wt.% PVA (Sigma–Aldrich, 99+ %, hydrolyzed) was dissolved in distilled water at 60 °C with stirring, and the solution was cooled down to room temperature. The prepared n-Si/MgO composite powder was put into PVA solution and stirred for 5 min. This Si/MgO/PVA solution subjected to a centrifuge process 5 times at 4500 rpm for 10 min, and dried in a vacuum oven at 60 °C for 24 h. For the carbonization of PVA, dried Si/MgO/PVA was pyrolyzed at 750 °C for 3 h under Ar atmosphere. The obtained Si/MgO/C powder was treated with 12 wt.% dilute HCl solution for 1 h, and 1.1 wt.% dilute HF solution for 10 min, and then washed and dried.

2.2. Electrochemical measurements

The test electrodes consisted of the active powder material (70 wt.%), carbon black (Ketjen Black, 10 wt.%) as a conducting agent, and poly amide imide (PAI, 20 wt.%) dissolved in *N*-methyl pyrrolidinone (NMP) at 60 °C as a binder. Each component was well mixed to form a slurry using a magnetic stirrer. The slurry was coated onto a copper foil substrate, pressed, and dried at 200 °C for 4 h under vacuum. Mass loading of tested electrodes was about 0.8 mg cm^{-2}. A coin-type electrochemical cell was used with Li foil as the counter and reference electrodes, and $LiPF_6$ (1 M) and fluoro ethylene carbonate (10%, FEC) in ethylene carbonate (EC)/diethyl carbonate (DEC) (3:7 (v/v), PANAX) as the electrolyte. The cell assembly and all of the electrochemical tests were carried out in an Ar-filled glove box. The cycling experiments were galvanostatically performed using a Maccor automated tester at various currents for the active material, within a voltage range between 0.05 and 1.5 V (*vs.* Li/Li^+). During the discharging step, Li was inserted into the electrode, and extracted from the electrode during charging.

2.3. Characterization

Investigation of the crystal structure was conducted using an X-ray diffractometer (XRD, Rigaku, D-MAX2500-PC) with Cu-Kα radiation. The morphology of the powdered samples was observed using a FESEM (JEOL, JSM-7401). The morphology, size, and SAED patterns of the powdered samples were observed using TEM (JEOL, JEM-2100F) with EDS mapping (EDS, Oxford). The BET (ASAP 2010 Analyzer) surface area was determined from the nitrogen adsorption–desorption isotherm by the BJH (Barrett–Joyner–Halenda) method. The Raman spectra were collected at room temperature with a Raman microscope (HORIABA Jobin Yvon, T64000), using an Ar laser with a wavelength of 514 nm as the excitation source. *Ex situ* XRD was employed to observe the structural changes occurring in the active material during the cycling. To prepare the *ex situ* XRD samples, the electrodes were detached from the coin-type electrochemical cell, washed with diethyl carbonate (DEC), dried for 3 h in an Ar-filled glove box, and coated with Kapton tape, which served as a protective film.

3. Results and discussion

Fig. 1A shows a schematic illustration of the fabrication process of the n-Si/C mesoporous composite. n-Si/MgO composite powder prepared by Mg_2Si reduction of a-SiO_2 using the HEMM process is coated with carbon matrix through a simple PVA coating and carbonization process. Finally, n-Si/C mesoporous composite is

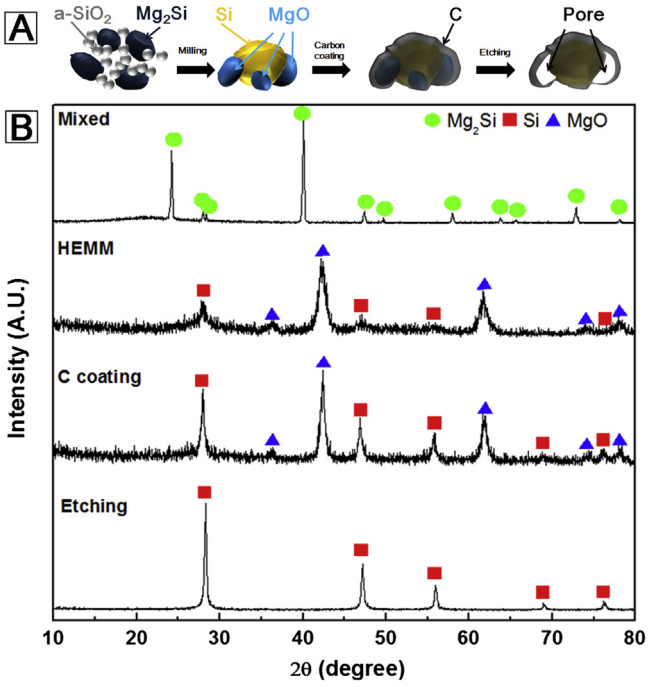

Fig. 1. (A) Schematic illustration of the fabrication process of n-Si/C mesoporous composite, (B) XRD patterns at each step for the fabrication of n-Si/C mesoporous composite.

obtained *via* chemical etching processes to eliminate MgO nano-particles (HCl etching), which act as pore generating agents for the formation of mesopores in the carbon matrix, as well as to remove any residual a-SiO_2 (HF etching). X-ray diffraction (XRD) patterns of the products at each step during the fabrication of n-Si/C mesoporous composite are shown in Fig. 1B. As shown in the XRD patterns, a-SiO_2/Mg_2Si composite (Mg_2Si: JCPDS No. 34-0458) is transformed into a n-Si/MgO composite (Si: JCPDS No. 01-0787; MgO: JCPDS No. 04-0829) after the HEMM process (Eq. (2)). The crystallite sizes of Si and MgO obtained using Scherrer's equation are approximately 11.1 nm and 13.2 nm, respectively. After the carbon coating process with PVA, the crystalline Si and MgO peaks become stronger and sharper compared with those of the n-Si/MgO composite. The calculated crystallite sizes of Si and MgO in the n-Si/MgO/C composite are 71.4 nm and 23.2 nm, respectively. The grain growth of Si and MgO phases are mainly due to exposure to temperature at 750 °C during the PVA carbonization process. In the XRD pattern of the n-Si/C mesoporous composite, only crystalline Si peaks are observed, since the crystalline MgO is completely removed through the etching process. The calculated crystallite size of Si is 89.2 nm.

The carbonization temperature (750 °C) for PVA is determined by referring to the previous research reported on nano-Si/C core–shell anode material for LIBs, since the conductivity of Si nano-particles coated by carbonized PVA at 750 °C is two orders of magnitude higher than that of nano-Si according to AC impedance measurements [18]. The Raman spectra for carbonized PVA at 750 °C under Ar atmosphere (Fig. 2A) and for the n-Si/C mesoporous composite (Fig. 2B) exhibit two Raman shifts near 1377 cm^{-1} and 1588 cm^{-1}, which are related to disordered carbon (D band) and graphitic carbon (G band), respectively. These results confirm the presence of the C matrix in the n-Si/C mesoporous composite. The presence of G band does not necessarily indicate the presence of long-range-ordering graphite domains in the carbonized PVA [33,34], and no peaks corresponding to graphite are observed in the XRD patterns of carbonized PVA, although graphite could help to enhance the electrical conductivity of the materials [33,34].

The morphology of n-Si/C mesoporous composite is observed by field emission scanning electron microscope (FESEM), and the results show that the particle size of n-Si/C mesoporous composite is in the range of 50 nm^{-1} μm (Fig. 2C). To demonstrate the porous nature of the n-Si/C mesoporous composite, Brunauer–Emmett–Teller (BET) surface area measurement from the nitrogen adsorption–desorption isotherm at 77 K is carried out (Fig. 2D). The BET surface area and the total pore volume at P/P_0 = 0.97 are 4.49 m^2 g^{-1} and 0.03 cm^3 g^{-1} for the n-Si/MgO/C composite, while those of the n-Si/C mesoporous composite are 151.25 m^2 g^{-1} and 0.61 cm^3 g^{-1}, respectively. The BET surface area and total pore volume are significantly increased after the elimination of the MgO phase through the HCl etching process, and a typical Type IV isotherm with a relatively large adsorption–desorption isotherm hysteresis of the n-Si/C mesoporous composite is also observed, which indicated capillary condensation of the gas in the meso- and macropores.

High-resolution transmission electron microscopy (HRTEM) with energy dispersive spectroscopy (EDS) mapping analyses for Si/MgO, Si/MgO/C, and n-Si/C mesoporous composite are conducted, and the results are shown in Fig. 3. Selected area energy dispersion (SAED) patterns of the n-Si/MgO composite (Fig. 3A) coincide with the XRD patterns (Fig. 1B). As shown in Fig. 3B, the n-Si/MgO composite particles (dark region) are surrounded by carbon matrix (bright region), and the SAED pattern still indicates the existence of Si and MgO phases. In contrast, the morphology of the n-Si/C mesoporous composite (Fig. 3C) shows a porous nature within the particles compared with the n-Si/MgO/C composite (Fig. 3B), since the meso-pores are formed by the elimination of MgO nano-particles embedded in the carbon matrix through the etching process. The elimination of MgO is confirmed by the SAED pattern, which shows that only Si remained. Thickness of carbon layer on Si particles is approximately 20 nm which is shown in Fig. 3D. The results of elemental mapping analyses using EDS show the distribution of elements or meso-pores more visually (the dotted square regions in Fig. 3A–C indicate the EDS mapping area). In the case of the n-Si/MgO (Fig. 3E) and n-Si/MgO/C (Fig. 3F) composites, Si and MgO nano-particles are clearly distinguishable (Mg: red region, Si: cyan region and C: dark blue region), and the existence of the carbon matrix can be observed in EDS mapping images of the n-Si/MgO/C composite. In the EDS mapping image of the n-Si/C mesoporous composite (Fig. 3G), the Mg region (red) disappears, and meso-pores are clearly observed in the EDS mapping image of the n-Si/C mesoporous composite (Fig. 3G). This observed meso-porous structure agrees well with the results of BET analyses.

Electrochemical cell tests are performed, and the results are shown in Fig. 4. The voltage profiles of n-Si/C mesoporous composite electrode (Fig. 4A) cycled between 0.05 and 1.5 V at a current of 0.4 A g^{-1} shows the characteristic shape of the Si electrode, representing the reaction of the crystalline Si electrode with Li at low potential. The discharge (lithiation) and charge (delithiation) capacities of the n-Si/C mesoporous composite electrode at the first cycle are 3050 mAh g^{-1} and 1867 mAh g^{-1}, respectively. The first discharge capacities of the n-Si/C mesoporous composite electrode do not reach the theoretical capacity ($Li_{15}Si_4$, 3600 mAh g^{-1} at room temperature), because the n-Si/C mesoporous composite electrodes are not lithiated below 0.05 V. The electrode can accommodate more Li ions, and transforms the amorphous Li–Si binary phase into crystalline $Li_{15}Si_4$. The absence of the crystalline $Li_{15}Si_4$ phase at 0.05 V is demonstrated by *ex situ* XRD analyses of the n-Si/C mesoporous composite electrode at the selected potential, which is indicated in the differential capacity plot (DCP) at the first cycle (Fig. 4B, inset: *ex situ* XRD patterns). There are no peaks related to Si

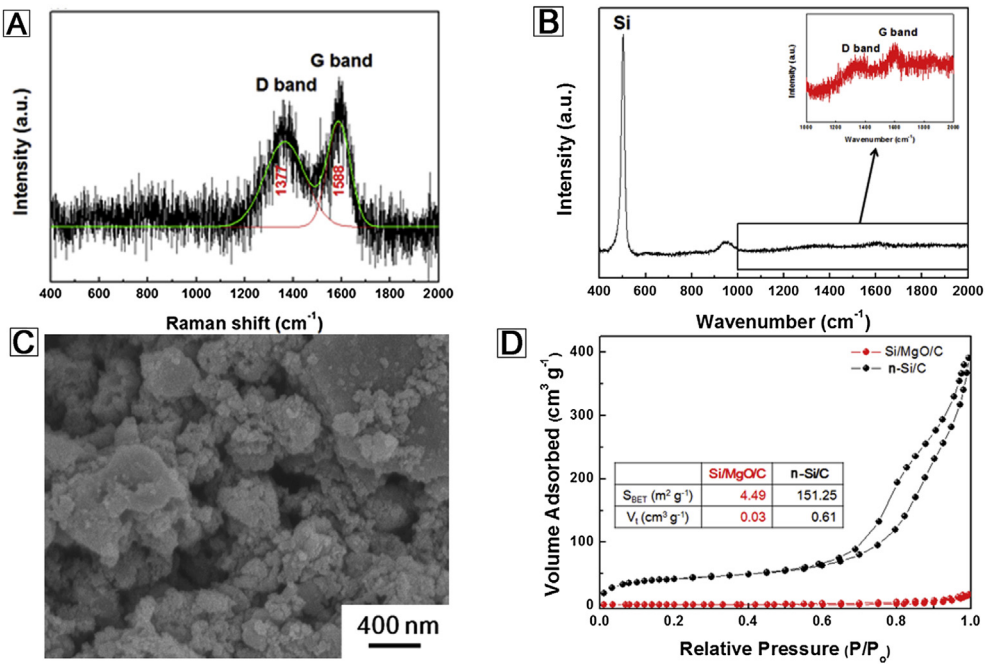

Fig. 2. Raman spectra of (A) carbonized PVA at 750 °C under Ar atmosphere and (B) n-Si/C mesoporous composite. (C) FESEM image of n-Si/C mesoporous composite. (D) A N_2 adsorption and desorption isotherm of n-Si/MgO/C and n-Si/C mesoporous composite.

or the Li–Si binary phase when the electrode is lithiated to 0.05 V. The crystalline Si peak of the decomposed Li–Si binary phase is not observed when the electrode is fully delithiated to 1.5 V, because of the solid-state amorphization phenomenon [35]. The n-Si/C mesoporous composite electrode is tested at a current of 0.2 A g^{-1} for the first 3 cycles and at a high current of 1.0 A g^{-1} for all subsequent cycles, and the results are presented in Fig. 4C. The n-Si/C mesoporous composite electrode exhibits excellent cycle performance with a reversible capacity of *ca.* 1600 mAh g^{-1} over 50 cycles at a high current of 1.0 A g^{-1} with the first Coulombic efficiency of 66%. The excellent cycle performance of the n-Si/C mesoporous composite electrode is mainly due to the meso-pores within the carbon matrix acting as buffering media against the volume change of the Si particles during the lithiation/delithiation process, also by enhancing the electrical conductivity of the electrode. The voltage cut-off up to 0.05 V also helps to exhibit good cyclability due to the limited reaction of Si with Li, which leads to a relatively low volume expansion during cycling. The n-Si/C mesoporous composite electrode also shows an excellent rate capability, as shown in Fig. 4D. A rate capability test is conducted in the potential range of 0.05–1.5 V,

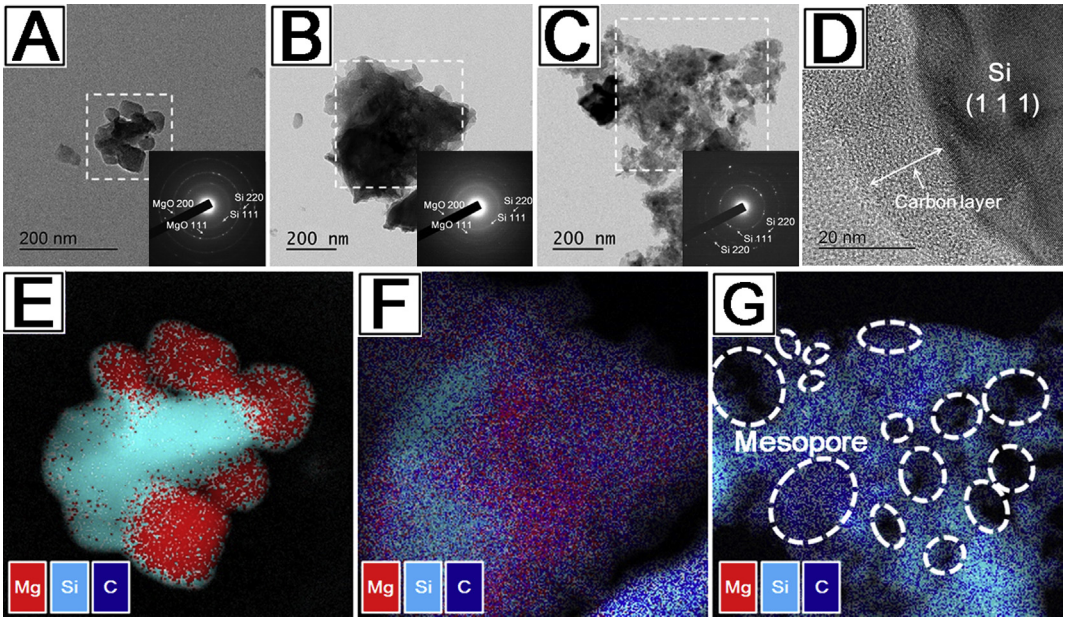

Fig. 3. TEM images with SAED patterns of (A) n-Si/MgO, (B) n-Si/MgO/C and (C) n-Si/C mesoporous composite, respectively (Highlighted region: EDS mapping area). (D) High resolution TEM image of n-Si/C mesoporous composite. EDS mapping images of (E) n-Si/MgO, (F) n-Si/MgO/C and (G) n-Si/C mesoporous composite.

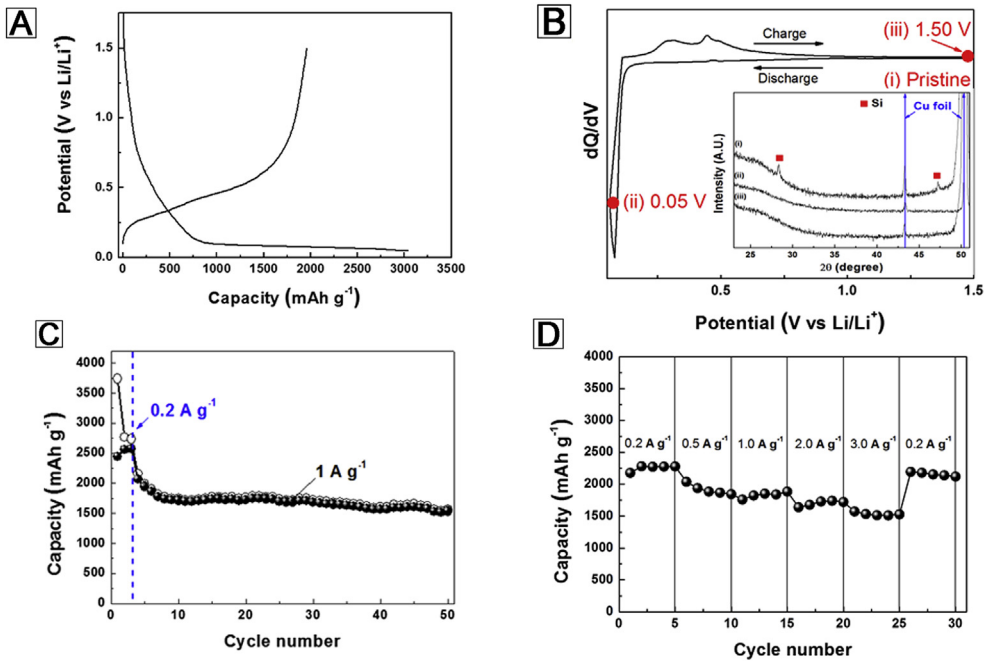

Fig. 4. The results of electrochemical cell test. (A) Voltage profiles of n-Si/C mesoporous composite electrodes at a current of 0.4 A g^{-1}. (B) DCP of the n-Si/C mesoporous composite electrode. (inset: *Ex situ* XRD patterns at selected potentials as indicated in DCP. (i) Pristine, (ii) lithiated to 0.05 V and (iii) delithiated to 1.5 V at the current of 0.4 A g^{-1}). (C) Cyclability of n-Si/C mesoporous composite electrode at a current of 0.2 A g^{-1} for the first 3 cycles and at a current of 1.0 A g^{-1} for subsequent cycles. (D) Rate capability test of n-Si/C mesoporous composite electrode at various current.

and the applied current at the charge step is fixed at 0.2 A g^{-1}. The original capacity at a discharge current of 0.2 A g^{-1} is almost 2300 mAh g^{-1}, and the electrode shows a large original capacity of 1530 mAh g^{-1}, even though the discharge current is increased to 3.0 A g^{-1}. After the discharge current returns to 0.2 A g^{-1}, the original capacity of the electrode is recovered to ca. 2200 mAh g^{-1}. The improved electrochemical properties are attributed to the unique nano-structure with the Si nano-particles being surrounded by the mesoporous carbon matrix, which supports the electrical contact between the Si particles, and alleviates the stress caused by the volume change during cycling. These excellent electrochemical properties are comparable to other previous researches on Si/C composite system [11–19].

4. Conclusions

The n-Si/C mesoporous composite as an anode material for LIBs is prepared facilely by the Mg_2Si reduction of a-SiO_2 using the HEMM process, simple carbon coating with PVA, and chemical etching of the MgO, in sequence. This n-Si/C mesoporous composite electrode shows excellent electrochemical performance as an anode for lithium ion batteries, achieving a reversible capacity greater than 1600 mAh g^{-1} over 50 cycles at a high current of 1.0 A g^{-1}, as well as superior rate capabilities with a reversible capacity of about 1530 mAh g^{-1} at a discharge current of 3 A g^{-1}. These excellent electrochemical properties of the n-Si/C mesoporous composite electrode are achieved by the mesoporous carbon matrix, which not only buffers the volume expansion of the silicon particles during the cycling, but also acts as a stable electrical conducting pathway.

References

[1] C.M. Park, Y.U. Kim, H. Kim, H.J. Sohn, Chem. Soc. Rev. 39 (2010) 3115–3141.
[2] C.J. Wen, R.A. Huggins, J. Solid State Chem. 37 (1981) 271–278.
[3] M.N. Obrovac, L. Christensen, Electrochem. Solid State Lett. 7 (2004) A93–A96.
[4] C.K. Chan, R.N. Pater, M.J. O'Connell, B.A. Korgel, Y. Cui, ACS Nano 4 (2010) 1443–1450.
[5] K. Evanoff, J. Khan, A.A. Balandin, A. Magasinski, W.J. Ready, T.F. Fuller, G. Yushin, Adv. Mater. 24 (2012) 533–537.
[6] H. Kim, B. Han, J. Choo, J. Cho, Angew. Chem. Int. Ed. 47 (2008) 10151–10154.
[7] M. Ge, J. Rong, X. Fang, C. Zhou, Nano Lett. 12 (2012) 2318–2323.
[8] H. Wu, G. Chan, I. Ryu, Y. Yao, M.T. McDowell, S.W. Lee, A. Jackson, Y. Yang, L. Hu, Y. Cui, Nat. Nanotechnol. 7 (2012) 310–315.
[9] A. Magasinski, P. Dixon, B. Hertzberg, A. Kvit, J. Ayala, Yushin, Nat. Mater. 9 (2010) 353–358.
[10] Y. Hwa, W.-S. Kim, B.-C. Yu, H. Kim, S.H. Hong, H.J. Sohn, J. Mater. Chem. A 1 (2013) 3733–3738.
[11] D.M. Piper, T.A. Yersak, S.-B. Son, S.C. Kim, C.S. Kang, J.H. Oh, C. Ban, A.C. Dillon, S.H. Lee, Adv. Energy Mater. 3 (2013) 697–702.
[12] Y.-S. Hu, R. Demir-Cakan, M.N. Titirici, J.O. Muller, R. Schlogl, M. Antonietti, J. Maier, Angew. Chem. Int. Ed. 47 (2008) 1645–1649.
[13] B. Hertzberg, A. Alexeev, G. Yushin, J. Am. Chem. Soc. 132 (2010) 8548–8549.
[14] M. Thakur, S.L. Sinsabaugh, M.J. Isaacson, M.S. Wong, S.L. Biswal, Sci. Rep. 20 (2012) 1–7.
[15] R. Yi, F. Dai, M.L. Gordin, S. Chen, D. Wang, Adv. Energy Mater. 3 (2013) 273.
[16] H. Wu, G. Yu, L. Pan, N. Liu, M.T. McDowell, Z. Bao, Y. Cui, Nat. Commun. 4 (2013) 1–6.
[17] N. Liu, H. Wu, M.T. McDowell, Y. Yao, C. Wang, Y. Cui, Nano Lett. 12 (2012) 3315.
[18] Y. Hwa, W.-S. Kim, S.-H. Hong, H.-J. Sohn, Electrochim. Acta 71 (2012) 201–205.
[19] D.S. Jung, T.H. Hwang, S.B. Park, J.W. Choi, Nano Lett. 13 (2013) 2092–2097.
[20] F. Han, W.-C. Li, M.-R. Li, A.-H. Lu, J. Mater. Chem. 22 (2012) 9645–9651.
[21] H. Zhou, S. Zhu, M. Hibino, I. Honma, M. Ichihara, Adv. Mater. 15 (2003) 2107–2111.
[22] S.H. Joo, S.J. Choi, I. Oh, J. Kwak, Z. Liu, O. Terasaki, R. Ryoo, Nature 412 (2001) 169–173.
[23] K.T. Lee, X. Ji, M. Rault, N.F. Nazar, Angew. Chem. Int. Ed. 48 (2009) 5661–5665.
[24] C. Suryanarayana, in: W.B. Eisen, B.L. Ferguson, R.M. German, R. Iacocca, P.W. Lee, D. Madan, K. Moyer, H. Sanderow, Y. Trudel (Eds.), ASM Handbook, ASM International, 1998, pp. 80–90.
[25] H. Ishihara, S. Mizutani, H. Inoue, US Pat. 0115734, 2006, http://www.sony.net/SonyInfo/News/Press/200502/05-006E/index.html.
[26] Y. Hwa, W.S. Kim, B.-C. Yu, S.-H. Hong, H.-J. Sohn, Energy Technol. 1 (2013) 327–331.
[27] Y. Yu, L. Gu, C. Zhu, S. Tsukimoto, P.A. van Aken, J. Maier, Adv. Mater. 22 (2010) 2247–2250.
[28] D. Chen, X. Mei, G. Ji, M. Lu, J. Xie, J. Lu, J.Y. Lee, Angew. Chem. Int. Ed. 51 (2012) 2409–2413.
[29] J. Chen, H. Zhao, J. He, J. Wang, Rare Met. 30 (2011) 166–169.
[30] J.-K. Yoo, J. Kim, Y. Jung, K. Kang, Adv. Mater. 24 (2012) 5452–5456.

[31] Z. Bao, M.R. Weatherspoon, S. Shian, Y. Cai, P.D. Graham, S.M. Allan, G. Ahmad, M.B. Dickerson, B.C. Church, Z. Kang, et al., Nature 446 (2007) 172–175.
[32] A. Basch, B. Gollas, R. Horn, J.O. Besenhard, J. Appl. Electrochem. 35 (2005) 169–176.
[33] C. Julien, K. Zaghib, A. Mauger, M. Massot, A. Ait-Salah, M. Selmane, F. Gendron, J. Appl. Phys. 100 (2006) 063551-1–063551-7.
[34] M. Ramsteiner, J. Wagner, C. Wild, P. Koidl, J. Appl. Phys. 62 (1987) 729–731.
[35] P. Limthongkul, Y.I. Jang, Y.M. Chiang, J. Power Sources 119 (2003) 604–609.